

## **Lamb Wave Generation with Piezoelectric Wafer Active Sensors for Structural Health Monitoring**

Victor Giurgiutiu, PhD  
Mechanical Engineering Department, University of South Carolina  
Columbia, SC 29208, [victorg@sc.edu](mailto:victorg@sc.edu)

### **ABSTRACT**

The capability of embedded piezoelectric wafer active sensors (PWAS) to perform in-situ nondestructive evaluation (NDE) is explored. Theoretical developments and laboratory tests are used to prove that PWAS transducers can satisfactorily perform Lamb wave transmission and reception, pulse-echo, pitch-catch, and phased array functions of conventional ultrasonics thus opening the road for embedded ultrasonics. Subsequently, crack detection in an aircraft panel with the pulse-echo method is illustrated. For large area scanning, a PWAS phased array is used to create the embedded ultrasonics structural radar (EUSR). For quality assurance, PWAS self-tests with the electromechanical impedance method are discussed.

**Keywords:** structural health monitoring, probabilistic neural networks, active sensors, piezoelectric, aging aircraft, cracks, damage, faults, diagnostics, prognostics, PWAS, E/M impedance

### **1. INTRODUCTION**

Embedded nondestructive evaluation (NDE) is an emerging technology that will allow transitioning the methods of conventional ultrasonics to embedded systems structural health monitoring (SHM) such as those envisioned for the Integrated Vehicle Health Management (IVHM). SHM for IVHM- requires the development of small, lightweight, inexpensive, unobtrusive, minimally invasive sensors to be embedded in the airframe with minimum weight penalty and at affordable costs [1]. Such sensors should be able to scan the structure and identify the presence of defects and incipient damage.

Current ultrasonic inspection of thin wall structures (e.g., aircraft shells, storage tanks, large pipes, etc.) is a time consuming operation that requires meticulous through-the-thickness C-scans over large areas. One method to increase the efficiency of thin-wall structures inspection is to utilize guided waves (e.g., Lamb waves) instead of the conventional pressure waves [2,3,4]. Guided waves propagate along the mid-surface of thin-wall plates and shallow shells. They can travel at relatively large distances with very little amplitude loss and offer the advantage of large-area coverage with a minimum of installed sensors [5,6]. Guided Lamb waves have opened new opportunities for cost-effective detection of damage in aircraft structures [7], and a large number of papers have recently been published on this subject [8]. Traditionally, guided waves have been generated by impinging the plate obliquely with a tone-burst from a relatively large ultrasonic transducer [9]. Snell's law ensures mode conversion at the interface, hence a combination of pressure and shear waves are simultaneously generated into the thin plate. However, conventional Lamb-wave probes (wedge and comb transducers) are relatively too heavy and expensive to be considered for widespread deployment on an aircraft structure as part of a SHM system. Hence, a different type of sensors than the conventional ultrasonic transducers is required for the SHM systems.

## 2. PIEZOELECTRIC WAFER ACTIVE SENSORS – PWAS

In recent years, several investigators [10-12] have explored the generation of Lamb-waves with piezoelectric wafer active sensors (PWAS)[13]. PWAS are inexpensive, non-intrusive, un-obtrusive, and minimally invasive devices that can be surface-mounted on existing structures inserted between the layers of lap joints, or inside composite materials. Figure 1 shows an array of 7 mm square PWAS mounted on an aircraft panel, adjacent to rivet heads and an electric discharge machined (EDM) simulated crack. The minimally invasive nature of the PWAS devices is apparent. These PWAS weight around 68 mg, are 0.2 mm thick, and cost \$7. PWAS operated on the piezoelectric principle that couples the electrical and mechanical variables in the material (mechanical strain,  $S_{ij}$ , mechanical stress,  $T_{kl}$ , electrical field,  $E_k$ , and electrical displacement  $D_j$ ) in the form:

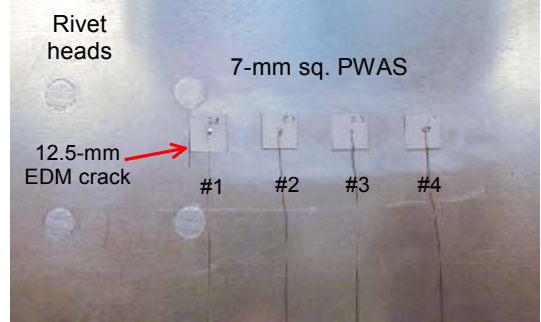


Figure 1 Piezoelectric wafer active sensors (PWAS) mounted on aircraft panel

$$\begin{aligned} S_{ij} &= s_{ijkl}^E T_{kl} + d_{kij} E_k \\ D_j &= d_{jkl} T_{kl} + \epsilon_{jk}^T E_k \end{aligned} \quad (1)$$

where  $s_{ijkl}^E$  is the mechanical compliance of the material measured at zero electric field ( $E = 0$ ),  $\epsilon_{jk}^T$  is the dielectric permittivity measured at zero mechanical stress ( $T = 0$ ), and  $d_{kij}$  represents the piezoelectric coupling effect. For embedded NDE applications, PWAS couple their in-plane motion, excited by the applied oscillatory voltage through the piezoelectric effect, with the Lamb-waves particle motion on the material surface. Lamb waves can be either quasi-axial ( $S_0, S_1, S_2, \dots$ ), or quasi-flexural ( $A_0, S_1, S_2, \dots$ ) as shown in Figure 2a,b. PWAS probes can act as both exciters and sensor of the elastic Lamb waves traveling in the material.

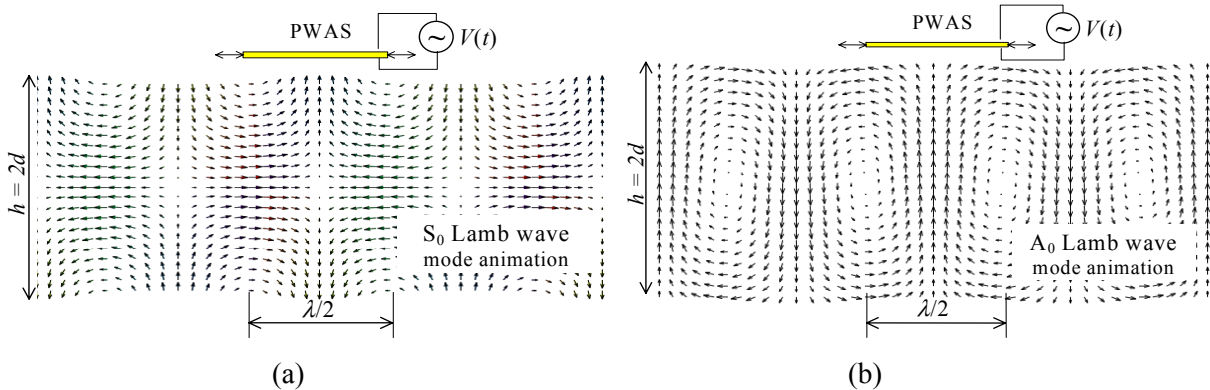


Figure 2 – PWAS interaction with Lamb modes: (a) symmetric Lamb mode  $S_0$ ; (b) anti-symmetric Lamb mode  $A_0$

For NDE, PWAS can be used as both active and passive probes. Thus, they address four IVHM-SHM needs [14-16]:

- 1) Far-field damage detection using pulse-echo and pitch-catch methods
- 2) Near-field damage detection using high-frequency impedance method
- 3) Acoustic emission monitoring of crack initiation and growth
- 4) Low-velocity impact detection

PWAS operation is different from that of conventional ultrasonic probes in the following aspects:

- 1) PWAS achieve Lamb wave excitation and sensing through surface “pinching” (in-plane strains), while conventional ultrasonic probes excite through surface “tapping” (normal stress).
- 2) PWAS are strongly coupled with the structure and follow the structural dynamics, while conventional ultrasonic probes are relatively free from the structure and follow their own dynamics.
- 3) PWAS are non-resonant wide-band devices, while conventional ultrasonic probes are narrow-band resonators.

The main advantage of PWAS over conventional ultrasonic probes lies in their small size, lightweight, low profile, and small cost. In spite of their small size, these novel devices are able to replicate many of the functions that the conventional ultrasonic probes, as proven by the proof-of-concept laboratory demonstrations described next.

### 3. LAMB MODE TUNED EXCITATION WITH PWAS TRANSDUCERS

The excitation of Lamb waves in plate with PWAS transducers is studied by considering the excitation applied by the PWAS through a surface stress  $\tau = \tau_0(x)e^{i\omega t}$ . Applying a space-domain Fourier transform analysis of the basic Lamb wave equations yields the strain wave and displacement wave solutions in the form:

$$\begin{aligned} \varepsilon_x(x,t) &= \frac{1}{2\pi} \frac{-i}{2\mu} \int_{-\infty}^{\infty} \left( \frac{\tilde{\tau} N_S}{D_S} + \frac{\tilde{\tau} N_A}{D_A} \right) e^{i(\xi x - \omega t)} d\xi \\ u_x(x,t) &= \frac{1}{2\pi} \frac{-i}{2\mu} \int_{-\infty}^{\infty} \frac{1}{\xi} \left( \frac{\tilde{\tau} N_S}{D_S} + \frac{\tilde{\tau} N_A}{D_A} \right) e^{i(\xi x - \omega t)} d\xi \end{aligned} \quad (2)$$

where  $\tilde{\tau}$  is the Fourier transform of  $\tau_a(x)$ ,  $p^2 = \frac{\omega^2}{c_L^2} - \xi^2$ ,  $q^2 = \frac{\omega^2}{c_T^2} - \xi^2$ , while  $c_L^2 = (\lambda + 2\mu) / \rho$  and  $c_T^2 = \mu / \rho$  are the longitudinal (pressure) and transverse (shear) wave speeds,  $\lambda$  and  $\mu$  are Lamé constants,  $\rho$  is the mass density, and

$$\begin{aligned} N_S &= \xi q (\xi^2 + q^2) \cos ph \cos qh, & D_S &= (\xi^2 - q^2)^2 \cos ph \sin qh + 4\xi^2 pq \sin ph \cos qh \\ N_A &= \xi q (\xi^2 + q^2) \sin ph \sin qh, & D_A &= (\xi^2 - q^2)^2 \sin ph \cos qh + 4\xi^2 pq \cos ph \sin qh \end{aligned} \quad (3)$$

Note that  $p$  and  $q$  depend on  $\xi$ , thus increasing the problem complexity. The integral in Equation (2) is singular at the roots of  $D_S$  and  $D_A$ . The equations  $D_S = 0$  and  $D_A = 0$  are exactly the Rayleigh-Lamb characteristic equations for symmetric and anti-symmetric motions accepting the simple roots:

$$\xi_0^S, \xi_1^S, \xi_2^S, \dots \quad \xi_0^A, \xi_1^A, \xi_2^A, \dots \quad (4)$$

corresponding to the symmetric (S) and anti-symmetric (A) Lamb waveguide modes. The evaluation of the integral in Equation (2) is done by the residue theorem, using a contour consisting of a semicircle in the upper half of the complex  $\xi$  plane and the real axis.

For ideal bonding between the PWAS and the plate, the shear stress in the bonding layer and the corresponding space-domain Fourier transform are:

$$\tau(x) = a\tau_0 [\delta(x-a) - \delta(x+a)], \quad \tilde{\tau} = a\tau_0 [-2i \sin \xi a] \quad (5)$$

Hence, the strain-wave solution becomes:

$$\varepsilon_x(x,t) = -i \frac{a\tau_0}{\mu} \sum_{\xi^S} \sin \xi^S a \frac{N_S(\xi^S)}{D'_S(\xi^S)} e^{i(\xi^S x - \omega t)} - i \frac{a\tau_0}{\mu} \sum_{\xi^A} \sin \xi^A a \frac{N_A(\xi^A)}{D'_A(\xi^A)} e^{i(\xi^A x - \omega t)} \quad (6)$$

Similarly, the displacement wave solution is obtained as:

$$u_x(x,t) = -i \frac{a\tau_0}{\mu} \sum_{\xi^S} \frac{\sin \xi^S a}{\xi^S} \frac{N_S(\xi^S)}{D'_S(\xi^S)} e^{i(\xi^S x - \omega t)} - i \frac{a\tau_0}{\mu} \sum_{\xi^A} \frac{\sin \xi^A a}{\xi^A} \frac{N_A(\xi^A)}{D'_A(\xi^A)} e^{i(\xi^A x - \omega t)} \quad (7)$$

**These expressions for Lamb wave response under PWAS excitation have not been published before.** A plot of these equations up to 1000 kHz is presented in Figure 3. Equations (6) and (7) contains the  $\sin \xi a$  behavior that displays maxima when the PWAS length  $l_a = 2a$  equals an odd multiple of the half wavelength, and minima when it equals an even multiple of the half wavelength. A complex pattern of such maxima and minima emerges, since several Lamb modes, each with its own different wavelength, coexist at the same time. Figure 3 shows the remarkable fact that, at 300 kHz, the amplitude of the  $A_0$  mode goes through zero, while that of the  $S_0$  is close to its peak. This represents an excitation “sweet spot” for  $S_0$  Lamb waves. Experimental results confirming this prediction are presented in Figure 3b.

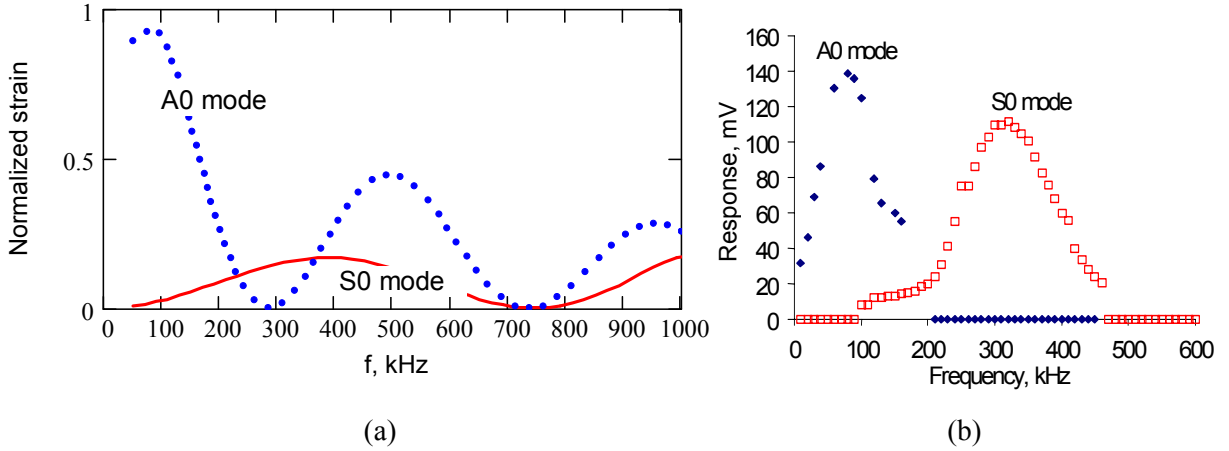


Figure 3 (a) Strain Lamb wave amplitudes predicted by the Lamb wave PWAS excitation tuning ( $S_0$  = continuous line;  $A_0$  = dotted line); (b) excitation sweet spot observed experimentally at 300 kHz in a 1.6-mm aluminum plate under a 7-mm PWAS excitation

This proves that frequencies can be found for which the response is dominated by certain preferentially excited modes. This is **wavelength-based mode tuning**. Another factor that must be considered in Lamb wave tuning under PWAS excitation is the mode amplitude at the plate surface. This factor is contained in the values taken for each mode by the function  $N/D'$ . Hence, it is conceivable that, at a given frequency, some higher modes may have less surface amplitudes, while other may have larger surface amplitudes. Thus, two important factors for the design of PWAS-based Lamb-wave embedded NDE for structural health monitoring have been identified:

- a) The variation of  $|\sin \xi a|$  with frequency for each Lamb wave mode
- b) The variation of the surface strain with frequency for each Lamb wave mode

Equations (6) and (7) can be viewed as a superposition of waveguide Lamb modes. In this case, the contribution of each mode in these equations can be expressed in the general form [6]:

$$A_{\xi}(x,t) = G \cdot E_{\xi} \cdot F \cdot e^{i(\xi x - \omega t)} \quad (8)$$

where  $G$  is a numerical factor representing the PWAS *transducer power* transmitted to the structure,  $E_{\xi}$  is the *excitability function* of mode  $\xi$ , and  $F$  is the *Fourier transform of the excitation*.

#### 4. PWAS GENERATED LAMB WAVES

The basic principles of Lamb wave generation and detection by PWAS probes were verified on simple laboratory experiments. A 1.6-mm thick, 2024-aluminum alloy rectangular plate (914mm x 504mm x 1.6 mm) was instrumented with eleven 7-mm sq., 0.2-mm thick PWAS (American Piezo Ceramics, APC-850) placed on a rectangular grid (Figure 4, Table 1). We verified that: (a) Lamb waves can be satisfactorily generated and detected with PWAS; (b) omnidirectional transmission is achieved; and (c) signals are strong enough and attenuation is sufficiently low for echoes to be detected. The proof of these attributes is especially important for Lamb wave excitation with PWAS, since these are at least an order of magnitude smaller and lighter than conventional ultrasonic transducers, and hence handle much less power.

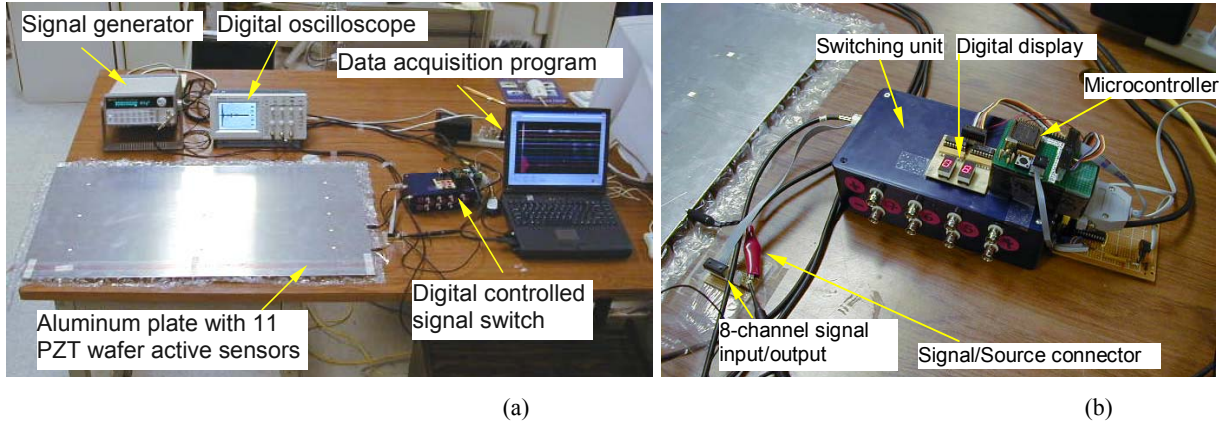


Figure 4 Experimental setup for rectangular plate wave propagation experiment: (a) overall view showing the plate, active sensors, and instrumentation; (b) detail of the microcontroller and switch box.

Table 1 Locations of sensors on the thin rectangular plate specimen

Sensor #	1	2	3	4	5	6	7	8	9	10	11
<b>x (mm)</b>	100	100	100	100	100	450	450	450	800	800	800
<b>y (mm)</b>	100	175	250	325	400	100	250	400	100	250	400

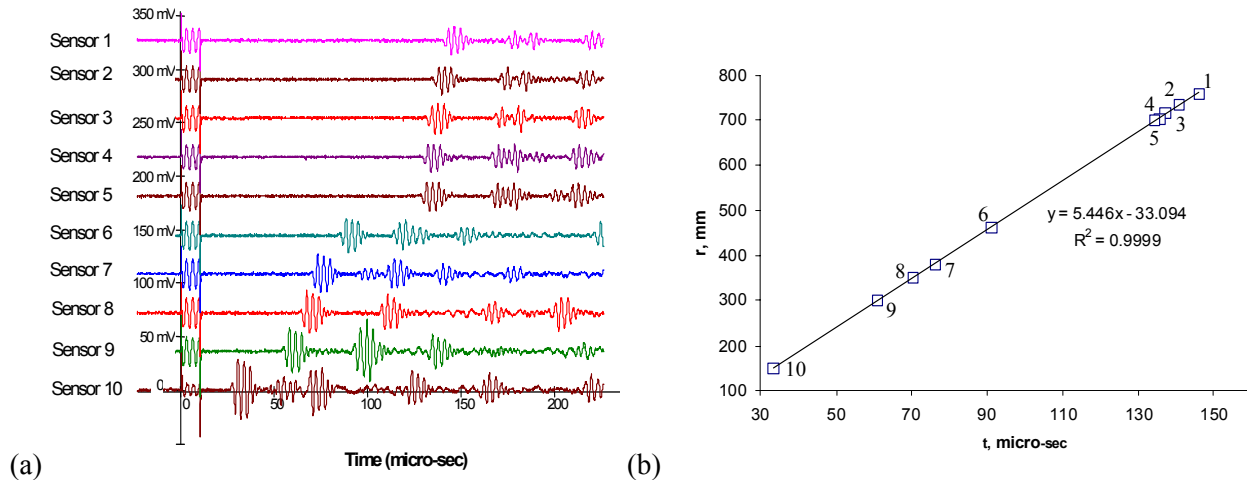


Figure 5 (a) Reception signals on active sensors 1 through 10; (b) correlation between radial distance and time of flight.

To prove that PWAS excite Lamb waves omnidirectionally, we used one PWAS (#11) as transmitter and the other PWAS (#1–10) as receivers. The signals observed in this investigation are shown in Figure 5a. Each row displays first the electromagnetically coupled ‘initial bang’ at the origin, then the wave packet

sent by the transmitter PWAS, followed by the wave packets resulting from boundary reflections at the plate edges. The time difference between the initial bang and the wave-package arrival represents the time-of-flight (TOF). The TOF is consistent with the distance traveled by the wave. Figure 5b shows the straight-line correlation between TOF and distance. The slope of this line is the experimental group velocity,  $c_g = 5.446$  km/s, vs. the theoretical value of 5.440 km/s. Very good accuracy was observed (99.99% correlation; 0.1% speed detection error). These experiments were repeated at various frequencies up to 600kHz. The experimental group velocities for symmetric and anti-symmetric Lamb waveguide modes were determined. When needed, PWAS transducers mounted in pairs on either side of the plate were used for exciting in phase for symmetric modes and in anti-phase for anti-symmetric modes. Very good correlation between the calculated and measured group velocities was observed for both symmetric and anti-symmetric Lamb modes, proving that:

- 1) PWAS-generated Lamb waves propagate are “loud and clear”
- 2) PWAS-generated Lamb waves propagate omnidirectionally
- 3) The measured group velocity of PWAS-generated Lamb wave correlates well with theory

### 5. PULSE-ECHO WITH PWAS

PWAS #11 was also used for the demonstration of pulse-echo capabilities. Figure 6a, which shows that the sensor #11 signal has two distinct zones: (i) the initial bang, during which the PWAS #11 acts as transmitter; and (ii) the echo zone, containing wave packets reflected by the plate boundaries and received back to PWAS #11. These echoes were processed to evaluate the pulse-echo capabilities of the method. Since the wave generated by the initial bang underwent multiple reflections from the plate edges, each of these reflections had a different path length, as shown in Figure 6b. It is interesting to note that the path lengths for reflections  $R_1$  and  $R_2$  are approximately equal. Hence, the echoes  $R_1$  and  $R_2$  in the pulse-echo signal of Figure 6a are almost superposed.

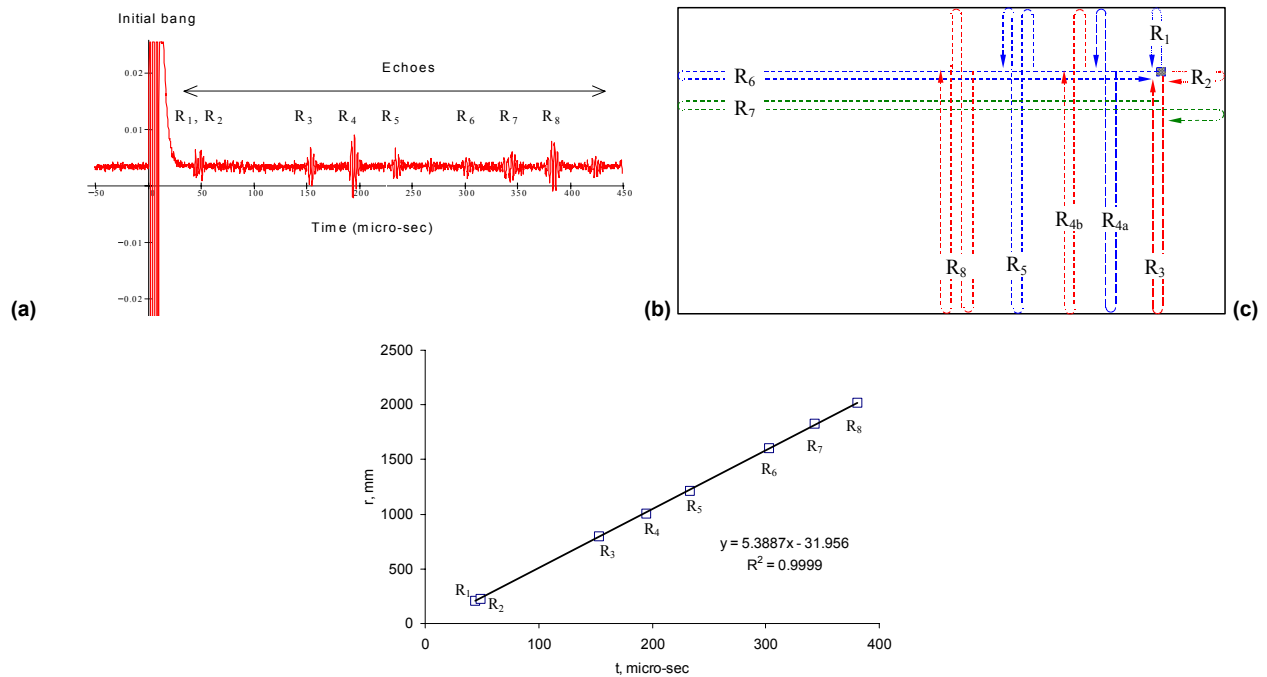


Figure 6 – Pulse-echo method applied to active sensor #11: (a) the excitation signal and the echo signals on active sensor 11; (b) schematic of the wave paths for each wave pack; (c) correlation of path length with time of flight.

Table 2 Analysis of pulse-echo signals of sensor #11 on rectangular plate specimen

Wave pack label	R <sub>1</sub>	R <sub>2</sub>	R <sub>3</sub>	R <sub>4</sub>	R <sub>5</sub>	R <sub>6</sub>	R <sub>7</sub>	R <sub>8</sub>
Time of flight (micro-sec)	43.8	48.8	152.8	194.4	233.2	302.8	343.2	380.8
Path length (mm)	104	114	400	504	608	800	914	1008

Also interesting to note is that the reflection R<sub>4</sub> has two possible paths of same length, R<sub>4a</sub> and R<sub>4b</sub>. Hence, the echoes corresponding to these two reflection paths arrive simultaneously and form a single but stronger echo, which has roughly twice the intensity of the other echoes. A plot of the TOF of each echo vs. its path length is given in Figure 6c. The straight line fit has a very good correlation ( $R^2 = 99.99\%$ ). The corresponding wave speed is 5.389 km/s, i.e., within 1% of the theoretical value of 5.440 km/s. The echoes were recorded from over 2,000 mm distance, which is remarkable for such small ultrasonic devices. Thus, it was proved that the PWAS are fully capable of transmitting and receiving pulse-echo signals of remarkable strength and clarity at relatively large distances.

## 6. CRACK DETECTION WITH PWAS

Wave propagation experiments were conducted on an aircraft panel to illustrate crack detection through the pulse-echo method. The panel had a typical aircraft construction, featuring a vertical splice joint and horizontal stiffeners. Figure 7 shows three photographs of PWAS installation on increasingly more complex structural regions of the panel. Adjacent to the photographs are the PWAS signals. All the experiments used only one PWAS, operated in pulse-echo mode. The PWAS was placed in the same relative location, i.e., at 200 mm to the right of the vertical row of rivets. The first row of Figure 7 shows the situation with the lowest complexity, in which only the vertical row of rivets is present in the far left. The signal to the right of this photograph shows the initial bang (centered at around 5.3 micro-sec) and multiple reflections from the panel edges and the splice joint. The echoes start to arrive at approximately 60  $\mu$ s. The second row of Figure 7 shows the vertical row of rivets in the far left and, in addition, a horizontal double row of rivets stretching towards the PWAS. The signal to the right shows that, in addition to the multiple echoes from the panel edges and the splice, the PWAS also receives backscatter echoes from the rivets located at the beginning of the horizontal row. These backscatter echoes are visible at around 42  $\mu$ s. The third row in Figure 7 shows a region of the panel similar to that presented in the previous row, but having an addition feature: a simulated crack (12.7-mm EDM hairline slit) emanating from the first rivet hole in the top horizontal row. The signal at the right of this photo shows features similar to those of the previous signal, but somehow stronger at the 42  $\mu$ s position. The features at 42  $\mu$ s correspond to the superposed reflections from the rivets and from the crack. The detection of the crack seems particularly difficult because the echoes from the crack and from the rivets are superposed.

This difficulty was resolved by using the differential signal method, i.e., subtracting the signal presented in the second row from the signal presented in the third row. In practice, such a situation would correspond to subtracting a signal previously recorded on the undamaged structure from the signal recorded now on the damaged structure. Such a situation of using archived signals is typical of health monitoring systems. When the two signals were subtracted, the result presented in the last row of Figure 7 was obtained. This differential signal shows a “loud and clear” echo due entirely to the crack. The echo, marked "reflection from the crack" is centered at 42  $\mu$ s, i.e., TOF = 37  $\mu$ s which correlates very well with a 5.4 km/s 200-mm total travel from the PWAS to the crack placed at 100 mm. The cleanness of the crack-detection feature and the quietness of the signal ahead of the crack-detection feature are remarkable. Thus, we concluded that PWAS are capable of clean and un-ambiguous detection of structural cracks.

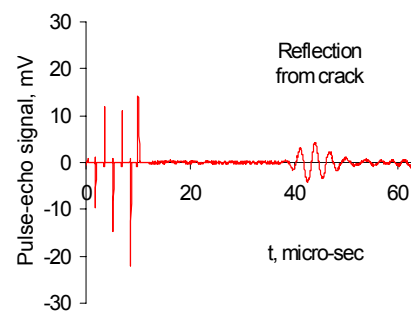
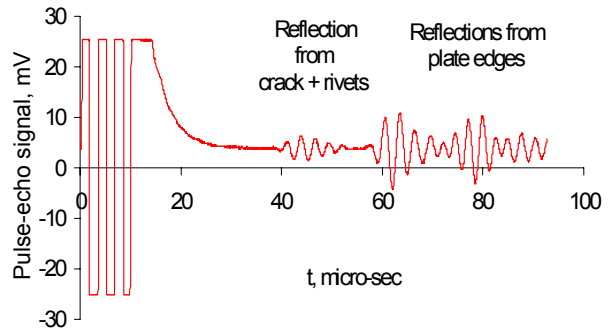
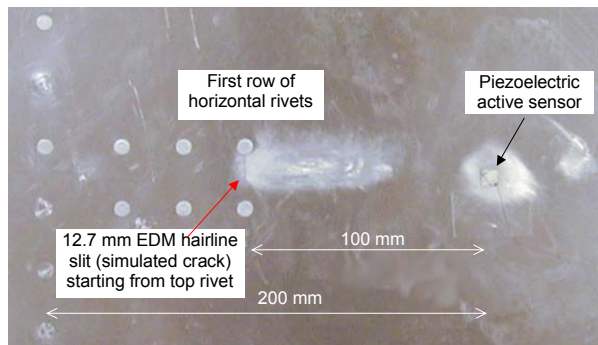
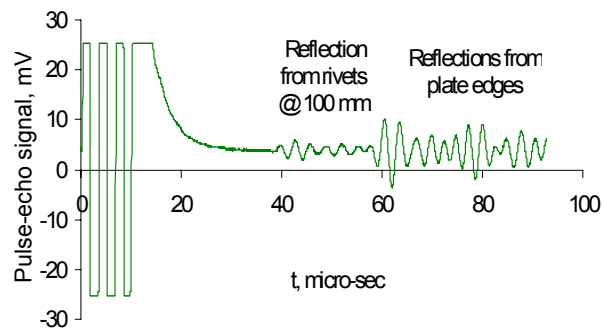
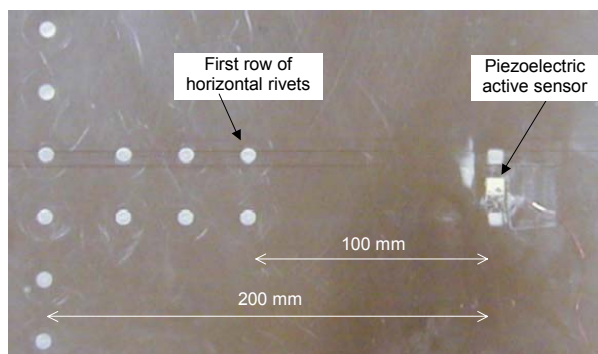
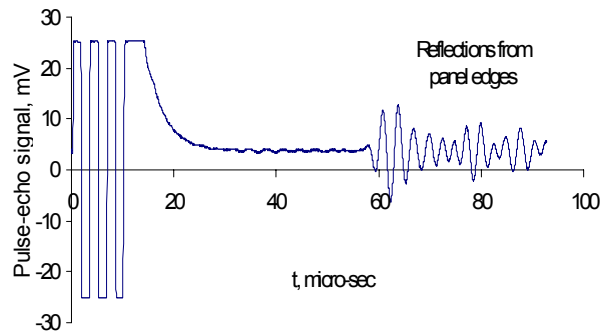
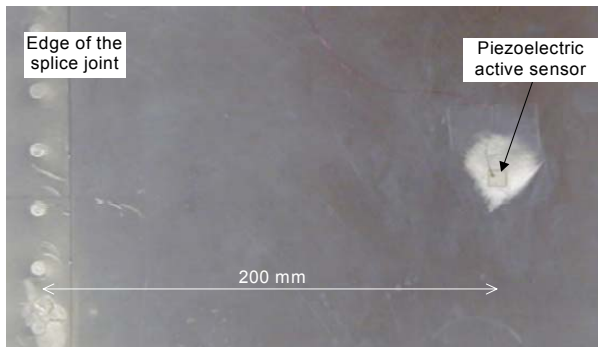


Figure 7 Crack-detection laboratory experiments on an aircraft panel: left column represents specimens (40-mil 2025 T3) with increasing complexity. Right column represents the pulse-echo signals. Fourth cell in the right column shows the crack detection through the differential signal method.



## 7. PWAS PHASED ARRAYS

The advantages of phased array transducers for ultrasonic testing are multiple [17,18]. Krautkramer, Inc. [19] produces a line of phased array transducers for the inspection of very thick specimens, and in the sidewise inspection of thick slabs, etc. These transducers employ pressure waves generated through normal impingement on the material surface. In our research [20, 21], we have developed a phased array technology for thin wall structures (e.g., aircraft shells, storage tanks, large pipes, etc.) that uses Lamb waves to cover a large surface area through beam steering from a central location. We called this concept *embedded ultrasonics structural radar* (EUSR) and constructed a simple proof-of-concept experiment (Figure 9a). A PWAS array was made up of a number of identical 7-mm sq. elements aligned at uniform 9-mm pitch. The PWAS phased array was placed at the center of a 4-ft square thin aluminum plate (Figure 9a). The wave pattern generated by the phased array is the result of the superposition of the waves generated by each individual element. By sequentially firing the individual elements of an array transducer at slightly different times, the ultrasonic wave front can be focused or steered in a specific direction. Thus, we achieved electronic sweeping and/or refocusing of the beam without physical manipulating the transducers. We proved that inspection of a wide zone is possible by creating a sweeping beam of ultrasonic Lamb waves that covered the whole plate. Once the beam steering and focusing was established, the detection of crack was done with the pulse-echo method. During these proof-of-concept experiments, the EUSR methodology was used to detect cracks in two typical situations: (i) a 19-mm broadside crack placed at 305 mm from the array in the 90 deg direction; and (ii) a 19-mm broadside crack placed at 409 mm from the array in the 136 deg direction. Of these two, the latter was more challenging because the ultrasonic beam is not reflected back to the source but rather deflected sideways. Hence, the echo received from the offside crack is merely the backscatter signal generated at the crack tips. Figure 9b presents the front panel of the embedded ultrasonic structural radar graphical user interface (EUSR-GUI) displaying the offside signals. The sweep is performed automatically to produce the structural defect image in the right pane. Manual sweep can be performed with the turn knob. The reconstructed signal is shown in the lower pane. In Figure 9b, the lower pane show the signal reconstructed at the beam angle  $\phi_0 = 136$  deg corresponding to the crack location. An animation of the crack detection methodology can be visualized using [click here](#) in Figure 9b.

## 8. PWAS SELF-TEST

Since the PWAS probes are adhesively bonded to the structure, the bond durability and the possibility of the probe becoming detached are of concern. To address this, we have identified a PWAS self-test procedure that can reliably determine if the sensor is still perfectly attached to the structure, or not. The procedure is based PWAS in-situ electromechanical impedance [14, 15]. Figure 8 compares the  $\text{Im } Z$  spectrum of a well-bonded PWAS with that of a disbonded (free) PWAS. The well-bonded PWAS presents a smooth  $\text{Im } Z$  curve, modulated by small structural resonances. The disbonded PWAS shows a strong self-resonance, and no structural resonances. The appearance of the PWAS resonance and the disappearance of structural resonances constitute features that can unambiguously discern when the PWAS has become disbonded, and can be used for automated PWAS self-test. For a partially disbonded PWAS, a mixture of PWAS and structure vibration was recorded.

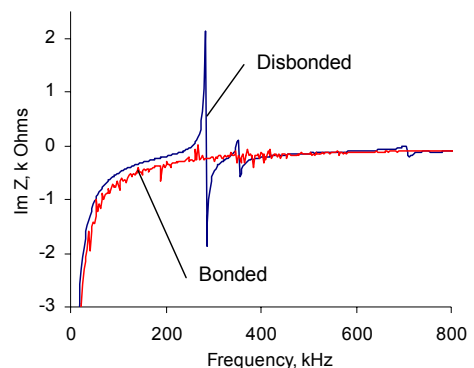
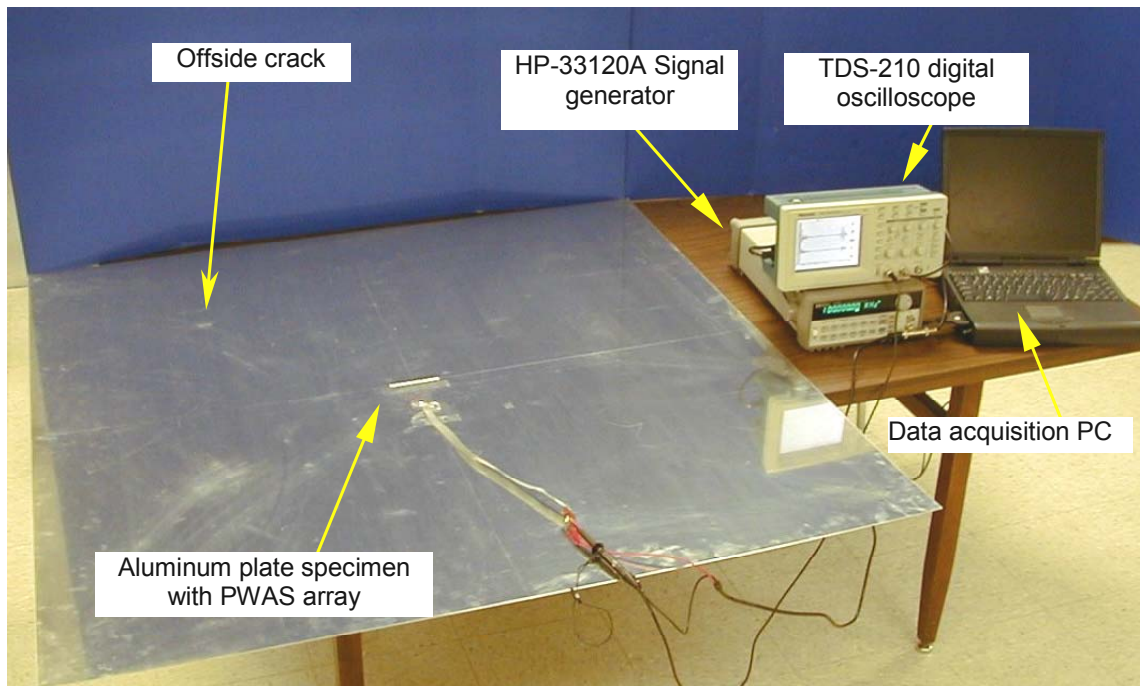
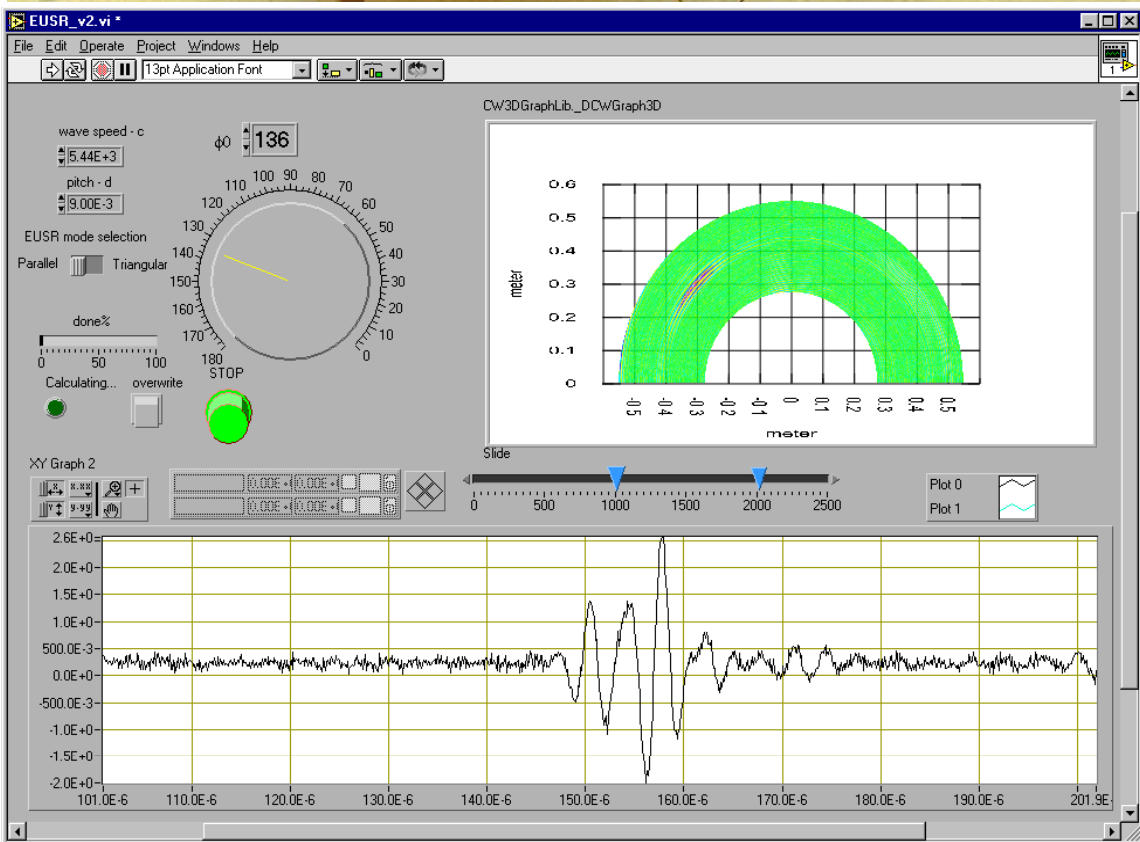


Figure 8 – PWAS self test: when sensor is disbonded, a clear free-vibration resonance appears at ~267 kHz



(a)



(b)

Figure 9 – Proof-of-concept EUSR experiment: (a) thin plate specimen 9-element PWAS array and 19-mm offside crack; (b) Graphical user interface (EUSR-GUI) front panel. The angle sweep is performed automatically to produce the structure/defect imaging picture on the right. Manual sweep of the beam angle can be also performed with the turn knob; the signal reconstructed at the particular beam angle (here,  $\phi_0 = 136$  deg) is shown in the lower picture.

## 9. SUMMARY AND CONCLUSIONS

A novel structural health-monitoring concept – embedded NDE with piezoelectric wafer active sensors (PWAS) has been presented. PWAS can be structurally embedded as both individual probes and as phased arrays. PWAS are inexpensive, non-intrusive, un-obtrusive, and minimally invasive devices that can be surface-mounted on existing structures inserted between the layers of lap joints, or inside composite materials. They can be placed inside closed cavities during fabrication/overhaul (such as wing structures or nuclear power plant piping), and then left in place for the life of the structure. The embedded NDE concept opens new horizons for performing in-situ damage detection and structural health monitoring of a multitude of thin-wall structures such as aircraft, spacecraft, missiles, pressure vessels, oil tanks, pipelines, etc. PWAS operation is different from that of conventional ultrasonic probes in the following aspects:

- 1) PWAS achieve Lamb wave excitation and sensing through surface “pinching” (in-plane strains), while conventional ultrasonic probes excite through surface “tapping” (normal stress)
- 2) PWAS are non-resonant wide-band devices, while conventional ultrasonic probes are narrow-band resonators
- 3) PWAS are strongly coupled with the structure and follow the structural dynamics, while conventional ultrasonic probes are relatively free from the structure and follow their own dynamics

The main advantage of PWAS over conventional ultrasonic probes lies in their small size, lightweight, low profile, and small cost. This paper has shown that, in spite of their small size, these novel transducers are able to replicate many of the functions that the conventional ultrasonic probes.

Theoretical developments have been presented, for the first time, that clarify the mechanism through which PWAS transducers can selectively excite various Lamb waveguide modes. The analysis was performed with the space-domain Fourier transform, and predicted both the displacement and strain Lamb waves. An excitation “sweet spot” for the  $S_0$  Lamb waveguide mode was predicted at around 300 kHz. This prediction was experimentally verified with remarkable accuracy.

Systematic experiments were conducted to verify that “loud and clear” ultrasonic Lamb waves can be successfully generated with the small, inexpensive, and unobtrusive PWAS transducers. Wave omnidirectionality and long distance propagation were proven. The pulse-echo crack-detection method was demonstrated on a simple plate specimen and on a realistic aircraft panel. The arrangement of PWAS in phased arrays was also explored. This resulted in the embedded ultrasonics structural radar (EUSR) concept, which opened additional opportunities for embedded NDE applications. The sweeping of a large structural area from a central location and the successful detection of broadside and offside cracks was demonstrated in a 1.2 m square plate. A graphical user interface (EUSR-GUI) was also presented.

The multiple-use capability of PWAS networks opens important opportunities for their use in smart vehicle structural health monitoring, damage detection, and failure prevention. The paper has examined how these opportunities address the Air Force vehicle structural health monitoring needs, and what areas of research need to be addressed in more depth. This emerging technology requires a sustained R&D effort to achieve its full developmental potential for applicability to full-scale aerospace vehicles.

## 10. ACKNOWLEDGMENTS

Partial support from the Department of Energy through the Sandia National Laboratories through contract doc. # BF 0133, from the National Science Foundation through grants NSF #CMS-9908293 and NSF INT-9904493, and participation in the US Air Force Summer Faculty Fellowship Program 2002 are thankfully acknowledged.

## 11. REFERENCES

1. Kropas-Hughes, C.V.; Perez, I.; Winfree, W. P.; Motzer, W. P.; Thompson, R. B. (2002) "Vision of Future Directions of NDE Research" in Review of Quantitative Nondestructive Evaluation Vol. 21, ed. by D. O. Thompson and D. E. Chimenti, American Institute of Physics, Vol. 615, 2002, pp. 2042-2051
2. Rose, J. L. (1995) "Recent Advances in Guided Wave NDE", *1995 IEEE Ultrasonics Symposium*, pp. 761-770
3. Krautkramer (1998) "Emerging Technology – Guided Wave Ultrasonics", *NDTnet*, Vol. 3, No. 6, June 1998.
4. Rose, J. L. (2002) "A Baseline and Vision of Ultrasonic Guided Wave Inspection Potential", *ASME Journal of Pressure Vessel Technology – Special Issue on Nondestructive Characterization of Structural Materials*, Vol. 124, No. 3, August 2002, pp. 273-282
5. Viktorov, I. A. (1967) *Rayleigh and Lamb Waves*, Plenum Press, New York, 1967
6. Rose, J. L. (1999) *Ultrasonic Waves in Solid Media*, Cambridge University Press, 1999
7. Dalton, R. P.; Cawley, P.; Lowe, M. J. S. (2001) "The Potential of Guided Waves for Monitoring Large Areas of Metallic Aircraft Structure", *Journal of Nondestructive Evaluation*, Vol. 20, pp. 29-46, 2001
8. Thomson, D. O. and Chimenti, D. E. (Editors) (2002) Review of Progress in Quantitative Nondestructive Evaluation, Chapter 2C "Guided Waves" and Chapter 7 "NDE Applications", *AIP Conference Proceedings* Vol. 615, 2002
9. Alleyne, D. N.; Cawley P. (1992) "Optimization of Lamb Wave Inspection Techniques", *NDTE International*, Vol. 25 (1992), No. 1, pp. 11–22
10. Keilers, C. H.; Chang, F.-K. (1995) "Identifying Delamination in Composite Beam using Built-in Piezoelectrics", *Journal of Intelligent Material Systems and Structures*, Vol. 6, 1995, pp. 647-672
11. Lin, X.; Yuan, F. G. (2001) "Diagnostic Lamb Waves in an Integrated Piezoelectric Sensor/Actuator Plate: Analytical and Experimental Studies", *Smart Materials and Structures*, Vol. 10, 2001, pp. 907-913
12. Giurgiutiu, V.; Zagrai, A. N.; Bao J.; Redmond, J.; Roach, D.; Rackow, K. (2002) "Active Sensors for Health Monitoring of Aging Aerospace Structures", *International Journal of the Condition Monitoring and Diagnostic Engineering Management*, UK, Vol. 5, No. 3, August 2002
13. Giurgiutiu, V.; Zagrai, A. (2000) "Characterization of Piezoelectric Wafer Active Sensors", *Journal of Intelligent Material Systems and Structures*, Technomic Pub., USA, Vol. 11, No. 12, December 2000, pp. 959-976
14. Giurgiutiu, V. (2001) In-situ Structural Health Monitoring, Diagnostics, and Prognostics System Utilizing Thin Piezoelectric Sensors, USC-IPMO Disclosure # 00284, 1/24/2001, U.S. Patent Office Application Serial No. 10–072,644 of February 8, 2002, Attorney Docket No. 16139/09021 (in process)
15. Giurgiutiu, V.; Zagrai, A. N. (2001) "Embedded Self-Sensing Piezoelectric Active Sensors for Online Structural Identification", *ASME Journal of Vibration and Acoustics*, Vol. 124, January 2001, pp. 116-125
16. Giurgiutiu, V.; Zagrai, A. N.; Bao, J. (2002) "Embedded Active Sensors for In-Situ Structural Health Monitoring of Thin-Wall Structures", *ASME Journal of Pressure Vessel Technology*, Vol. 124, No. 3, August 2002, pp. 293-302
17. Krautkramer, J.; Krautkramer, H. (1990) *Ultrasonic Testing of Materials*, Springer-Verlag, 1990
18. Lines D.; Dickson K. (1999) "Optimization of High-Frequency Array Technology for Lap-Joint Inspection"; *Proceedings of the 3<sup>rd</sup> Joint Conference on Aging Aircraft, 1999*, [www.galaxyscientific.com/agingaircraft/index2.htm](http://www.galaxyscientific.com/agingaircraft/index2.htm)
19. Krautkramer (2002), *Products Catalog*, <http://www.krautkramer.com/arrayweb/default.htm>
20. Giurgiutiu, V.; Bao, J. J. (2002) Embedded-Ultrasonics Structural Radar (EUSR) with Piezoelectric-Wafer Active Sensors (PWAS) for Wide-Area Nondestructive Evaluation of Thin-Wall Structures, USC-IPMO, Disclosure ID No. 00327 of 02/13/2002
21. Giurgiutiu, V.; Bao, J. (2002) "Embedded Ultrasonic Structural Radar for the Nondestructive Evaluation of Thin-Wall Structures" *Proceedings of the 2002 ASME International Mechanical Engineering Congress*, November 17-22, 2002, New Orleans, LA, paper # IMECE2002-39017